2026 IEEE International Conference on Robotics and Automation (ICRA 2026)
June 1-5, 2026. Vienna, Austria

# Colonial Architectures for Centimeter-Scale Underwater Robot Swarms

Pascal Spino[1,2], Marc Bäckert[1], Lianhao Yin[1], and Daniela Rus[1]

***Abstract*— Micro underwater robots offer scalable and low-cost access to environments that are difficult to study with conventional vehicles, but severe communication constraints, limited onboard power, and low swimming speed restrict the capability of these miniature systems. Inspired by colonial organisms such as salps and siphonophores, this work explores physically connected swarms of small underwater robots that form larger structures with improved collective performance. We present a modular platform of centimeter-scale robots capable of three-dimensional propulsion, onboard sensing, and autonomous behavior, with magnetic interfaces that enable reversible connections into prescribed morphologies. Experiments demonstrate autonomous assembly and disassembly, quantify the propulsive benefits of chain aggregates, and show that mechanically coupled robots can distribute sensing, actuation, and control across the collective. Results indicate that certain colonial architectures can greatly improve swimming speed, locomotion efficiency, and task performance compared to individual robots, suggesting a path toward more capable centimeter-scale underwater swarms.**

## I. INTRODUCTION

Micro underwater robots are a developing technology that may significantly extend our ability to monitor and explore aquatic environments [1]–[4]. These systems promise low-cost, scalable access to regions that are difficult to study with traditional vehicles such as shipwreck interiors and caves. However, unlike miniature robots that operate in air such as quadrotors, underwater robots cannot meaningfully offload sensing or computation to external systems due to the strong attenuation of electromagnetic signals in water and the bandwidth limits of other communication mediums like acoustic. These constraints are especially severe at small scales; micro underwater robots must carry all sensing, computation, and power onboard despite their limited volume, which restricts both capability and endurance. In addition, smaller swimmers typically exhibit lower propulsion efficiency [5], [6] and can carry only small batteries, further limiting their operational range. As a result, micro underwater robots have largely remained confined to laboratory settings. One path forward is to develop methods to coordinate swarms of micro robots such that they distribute sensing, computation, and locomotion across many units to achieve better performance. This raises a central question: what swarm morphologies enable capabilities that scale with the number of robots in underwater environments?

Nature provides one possible answer in colonial organisms such as salps and siphonophores. These millimeter- to centimeter-scale animals physically connect to form larger structures that behave collectively as a single organism. Colonial architectures produce measurable gains in both swimming speed and efficiency [7]–[10] while distributing sensing and decision-making across individuals [11], [12]. Colonies can also disassemble into solitary individuals when advantageous, effectively transforming one sophisticated organism into many smaller, simpler ones. Different colonial morphologies provide different functional benefits, with certain arrangements improving propulsion while others enhance sensing or feeding [13], [14].

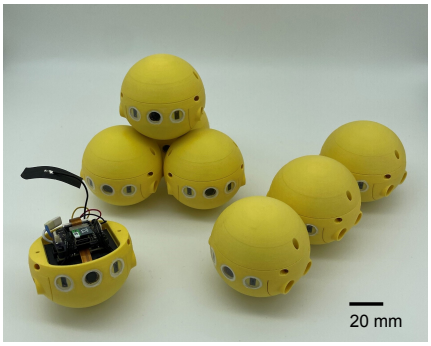


Fig. 1. A fleet of eight BμBL robots used in this work. Individual robots can connect by magnetic couplings to form chains or other topologies.

This paper explores bioinspired colonial architectures using a modular centimeter-scale underwater robot termed BμBL. Each BμBL unit is identical and independently capable of three-dimensional propulsion with onboard LiDAR, computer vision, pressure, and inertial sensing. A passive magnetic docking mechanism enables BμBL units to connect and disconnect in prescribed configurations. Using this platform, we study autonomous self-assembly and self-disassembly under constrained sensing and actuation, quantify the propulsive benefits of chain aggregates, and investigate how modular arrangements distribute actuation, sensing, and computation across a collective. This paper makes the following contributions:

- Design and implementation of a modular centimeter-scale underwater robot capable of autonomous self-assembly and self-disassembly.
- Quantification of how aggregate chain length affects steady-state swim speed and cost of transport.
- Demonstration of a station-keeping task in which identical local controllers, without inter-robot communication, achieve lower error when coupled as an aggregate compared to an individual.

[1]Computer Science and Artificial Intelligence Laboratory, Massachusetts Institute of Technology, Cambridge, MA, 02139, USA
[2]Department of Mechanical Engineering, Massachusetts Institute of Technology, Cambridge, MA, 02139, USA spino@mit.edu

### A. Underwater Swarms

Robot swarms offer a promising approach for underwater exploration by distributing sensing, actuation, and computation across many units. In contrast to single vehicles, swarms can achieve greater spatial coverage, parallel sensing, and robustness through redundancy, enabling tasks such as environmental monitoring, inspection, and exploration over larger areas. Recent work has begun to investigate swarming behaviors with small underwater robots, including centimeter-scale fish-like platforms designed for collective sensing and coordination [15], [16]. While these systems demonstrate the feasibility of underwater robot swarms, they have largely remained confined to controlled laboratory environments. A central open challenge is in identifying swarm architectures whose capabilities scale with the number of robots. For example, collective morphologies that improve sensing coverage, locomotion efficiency, or endurance as additional robots are added would significantly expand the practical utility of underwater swarms, but such scaling properties have not yet been demonstrated.

### B. Hierarchical Robots

Hierarchical robots—also referred to as modular self-reconfigurable robots or programmable matter—are robotic systems constructed from smaller modules whose sensing, actuation, and computation are distributed across the collective. By rearranging connectivity, the same modules can form different morphologies and therefore achieve multiple behaviors through self-assembly. Modules may be identical or specialized; in this work we consider identical underwater robots capable of operating independently. Early modular systems such as PolyBot [17] and Molecule [18] demonstrated reconfigurable assemblies of identical modules. Subsequent systems explored different geometries and docking mechanisms, including cube-based robots with magnetic alignment [19], [20], spherical robots with continuous surface connections [21], [22], and mobile docking robots capable of independent locomotion [23]–[27]. Hierarchical systems have also been studied for machine self-replication [28]–[30]. Despite this extensive work, most studies emphasize mechanisms and assembly rules rather than performance advantages of aggregates. With the exception of modular quadrotors [31], most systems remain terrestrial. Aquatic modular robots have only recently emerged, including modular boats [32], cubic underwater modules [33], [34], and salp-inspired soft robots [35]. Hierarchical architectures for centimeter-scale underwater robots remain largely unexplored.

### C. Bioinspiration: Salps

Salps are colonial marine organisms whose individual units typically range from $1\,\mathrm{cm}$ to $10\,\mathrm{cm}$ in length depending on species and life stage. Their lifecycle alternates between solitary and colonial forms. In the solitary stage, an individual salp swims using pulsed jet propulsion while feeding on suspended particles [36]. In the colonial stage, salps connect through specialized plaques to form aggregates that contain tens to hundreds of individuals [9]. These connections form strong mechanical bonds but can be actively released, allowing colonies to disassemble into solitary individuals [11]. Colonies take several forms across species, with the most studied configuration being the linear chains formed by *Salpa fusiformis* and related species [13]. Individuals within these chains coordinate their pulsed jetting through local interactions [11]. Colonial architectures provide two key advantages to the salp. First, swimming performance improves substantially: chain aggregates can travel much faster and with greater efficiency than solitary individuals [8]. This enables colonies to migrate efficiently to feeding grounds before dispersing into individuals that cover larger areas. Second, colony-level behavior emerges from local interactions without centralized control [9], [11]. Each salp contains its own propulsion, sensing organs, and simple nervous system, distributing sensing and decision-making across the colony. These properties closely parallel the goals of distributed autonomy in robotic collectives.

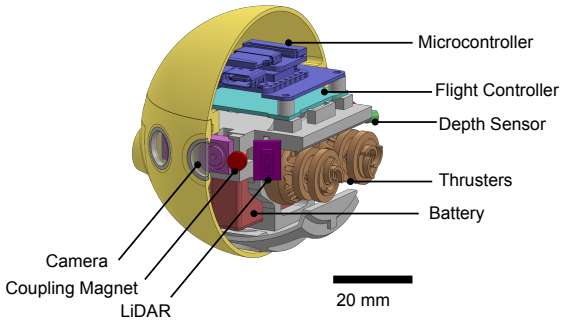


Fig. 2. Diagram of the BμBL robot with a cross section of the watertight shell. Each robot is equipped with four water jet propulsors and packed with a suite of sensors and small processors.

## II. Design

### A. Robot Architecture

The robot used in this study is a self-contained spherical underwater platform equipped with four fluid jet actuators that produce variable thrust, enabling three-dimensional propulsion and attitude control. The platform, termed BμBL, is shown in Figure 2. The propulsion system and control architecture were developed in prior work [37], [38]; here the platform is extended with a magnetic docking mechanism for multi-agent experiments. The robot measures $64\,\mathrm{mm}$ in diameter with a mass of $127\,\mathrm{g}$, and carries its own battery. During experiments it can be commanded wirelessly over Bluetooth low energy (BLE) and achieves swimming speeds up to $250\,\mathrm{mm/s}$ while regulating depth and attitude using its onboard controller. To support autonomous operation, the robot carries two multizone LiDAR sensors and a camera for perception, along with a six-axis IMU and pressure sensor for state estimation. The electrical power delivered to the propulsion system is also measured using onboard voltage and current meters, and all data is logged at $50\,\mathrm{Hz}$ to an onboard microSD card for post-experiment analysis.

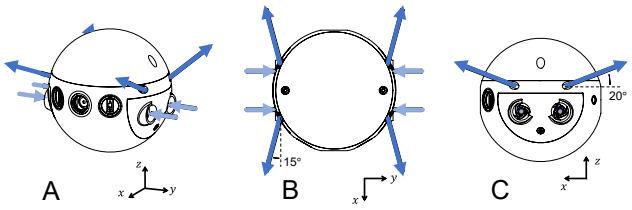


Fig. 3. Schematic of the BμBL propulsion system. The robot is equipped with four mirrored propulsors that resemble centrifugal pumps. Each propulsor intakes water from an inlet on the side of the vehicle (light blue) and expels it from a jet near the equator (dark blue); each jet is precisely angled 20° above the equatorial plane, and 15° to the side. The robot is controlled by regulating the flow rate of each jet. (A) isometric view. (B) top-down view, with the robot facing downwards. (C) side-view, with the robot facing left.

### B. Propulsion System

Locomotion is produced by four independently controlled water-jet propulsors arranged symmetrically around the equator of the BμBL. Each propulsor draws water through an inlet on the side of the vehicle and expels it through a narrow outlet, producing thrust proportional to the motor speed. In static tests each propulsor can generate up to $75\,\mathrm{mN}$ of thrust. By coordinating the four jets, the robot can generate body forces and torques to control forward motion, depth, roll, pitch, and yaw. The jet outlets are angled to reduce hydrodynamic interference between robots when operating in chain aggregates. This vector was tuned using the force measurement stand shown in Appendix Figure 13 to minimize downwash effects. Similar off-axis propulsion arrangements are observed in salp and siphonophore colonies [10], [39].

### C. Vision System

The BμBL vision system consists of an OV5640 camera processed by an ESP32S3 microcontroller. The camera views through the central window of the robot, which is aligned with its direction of forward motion. While the onboard multizone LiDAR sensors are limited to approximately $16\,\mathrm{cm}$ underwater range, the camera provides sensing at meter-scale distances in favorable optical conditions for relatively little mass ($\sim 2.4\,\mathrm{g}$). The onboard vision processing uses a low-compute color-based blob tracking algorithm running at up to $90\,\mathrm{Hz}$ with a $160 \times 120$ resolution image. The algorithm masks the camera frame to select all pixels of a desired color band, and then selects the largest connected region. The centroid of this region provides relative bearing to the target, while the region width provides a proxy for distance. Using this information, the robot performs visual servoing to approach and maintain position relative to colored objects. In this work, we use the vision system to identify and move towards other yellow robots, and to station-keep relative to red markers. The algorithm is implemented in C++.

### D. Docking Mechanism

The robot docking mechanism uses magnetism to passively align and maintain a preload between linked robots without consuming power. Each robot has two docking ports—one at the front and one at the rear—each consisting of two neodymium cylinder magnets $4.8\,\mathrm{mm}$ in diameter arranged with opposing polarity so that robots attract only when properly aligned. Experiments show that for inter-robot separations less than $9\,\mathrm{mm}$ and angular mismatch less than $20°$, the mechanism passively self-aligns and docks free-floating BμBL robots. The interface supports tensile loads up to $350\,\mathrm{mN}$, sufficient to maintain connection under maximum opposing thrust. BμBL robots can undock by coordinating their jet propulsors to apply opposing torques to create a separating torque at the interface. Figure 4 illustrates the docking mechanism and the resulting chain aggregates. The magnets are fully enclosed within the hull.

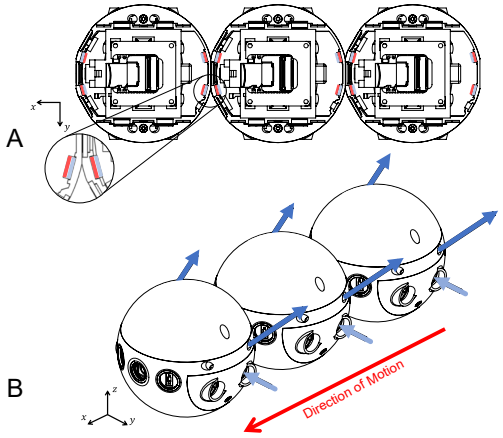


Fig. 4. (A) Top-down view of a chain of three docked robots, with cross-section of the shell to show the arrangement of internal docking magnets (colored red and blue to indicate polarity) (B) Isometric view of a chain of three docked robots showing the vectors of fluid jets from each robot and the resulting aggregate direction of motion.

### E. Communication

Each BμBL communicates bidirectionally with a base station over Bluetooth Low Energy (BLE) to receive commands and stream onboard data. BμBL robots are assigned unique identifiers for individual addressing. Due to strong electromagnetic attenuation in water, the BLE link is maintained only when BμBL robots are submerged less than $5\,\mathrm{cm}$; when disconnected, the robots behave autonomously until connection is re-established. This centralized communication architecture was used for experiments with up to eight robots. While inter-robot communication was not required for the experiments presented here, BμBL robots can exchange messages with docked neighbors, enabling communication across aggregates that will be explored in future work.

## III. Experiments

Three sets of experiments are performed in this work. The first set of experiments assess the ability of BμBL pairs to self-assemble and self-disassemble with only onboard sensing and actuation methods. The second set of experiments explores distributed propulsion in chain aggregates of the robots, which are linear structures associated with high

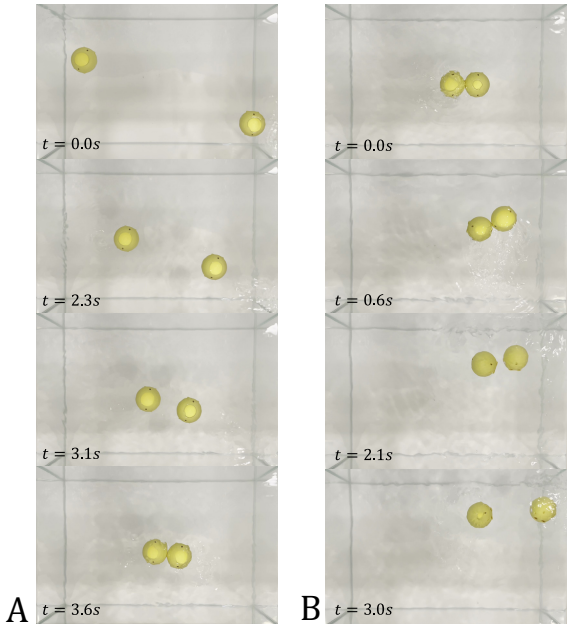


Fig. 5. (A) Sequence of self-assembly relying only on onboard vision and self-propulsion. The robots are initialized drifting in opposing corners of the tank. Once commanded, they rotate to search for another robot and then apply constant forward thrust while regulating their heading to eventually dock. (B) Sequence of self-disassembly. The robots apply maximum torques in opposite directions in order to overcome the holding force of the magnetic dock.

speed and efficiency in salp and siphonophore colonies [8]–[10]. These experiments investigate the scaling behavior for two strategies inspired by salps: in the first all robots in the chain produce thrust, and in the second only a single robot provides thrust while the other robots are passive. Experiments are performed with up to eight BμBL robots. The final set of experiments explores a task where the robots are commanded to station-keep relative to a marker via coordinating their vision system and propulsion. Through this experiment we show that groups of connected robots can achieve better performance than individuals even without any explicit communication between units.

Experiments are performed in two laboratory freshwater tanks. A $60\,\mathrm{cm} \times 40\,\mathrm{cm} \times 40\,\mathrm{cm}$ tank is used for assembly, disassembly, and station-keep experiments. A much larger $4\,\mathrm{m} \times 3\,\mathrm{m} \times 1\,\mathrm{m}$ tank is used for the aggregate chain propulsion experiments. In both cases, a downward-facing camera (GoPro 11 Black) is mounted above the center of the tank. The 2D robot trajectories are recovered from camera recordings through a combination of color tracking and edge tracking via MATLAB, which is calibrated to absolute length scale for each experiment.

### A. Self-Assembly

The self-assembly process utilizes the robot vision system and self-propulsion to close distance between BμBL robots and perform course heading alignment. The robots follow a simple control law to search for another yellow object and then to move directly towards it; when both robots execute this law, they eventually find and collide head-first with one another. Fine alignment and anchoring is performed passively by the magnetic docks as the robots collide, and no external tracking systems are used to aid in self-assembly. Figure 5(A) shows a sequence of two robots beginning at opposing corners of the laboratory tank, and autonomously self-assembling upon being commanded to do so. The magnetic dock is built from permanent magnets and does not consume power to maintain a holding force.

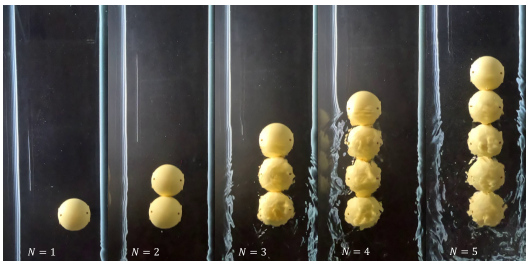


Fig. 6. Comparison of chain aggregates of the robots, from one to five robots. Frames are adapted from video captured mid-swim. As seen by the images, there is significantly more disturbance in the tank water as the number of robots is increased.

### B. Self-Disassembly

Figure 5(B) shows the disassembly sequence of two connected BμBL robots. The robots begin in a docked hovering mode and are commanded to apply disassembly maneuvers. This maneuver requires each robot produces maximum propulsive yaw torque in opposing directions. After a brief period ($0.6\,\mathrm{s}$ average across experiments) the robots break contact at the dock interface. After another brief period, the robots become fully separated. Each robot expends about $3.8\,\mathrm{J}$ to its propulsion system in order to disconnect, less than $0.1\,\%$ of its stored energy ($\sim 8\,\mathrm{kJ}$) and not much more energy than would be consumed over the same interval of regular hovering.

### C. Swimming in Chain Aggregates

A single BμBL robot with four independent propulsors and six degrees of freedom is underactuated, but a chain aggregate of BμBL robots becomes increasingly overactuated as robots are added. This is because the number of independent propulsors scales with the number of robots while the degrees of freedom of the aggregate remains constant. As a result, there are many propulsion strategies available to the chain aggregate; for example, some units may generate thrust while others remain passive. A similar phenomenon is observed in linear salp colonies, where swimming behavior varies with context. For example, all salps may thrust simultaneously when escaping predators, whereas only a subset may pulse during routine swimming. Motivated by this biological precedent, we evaluate propulsion strategies at two extreme ends of the spectrum. In the first strategy, all robots in the chain produce identical thrust. In the second, only a single robot—the rear robot in the chain—produces thrust while the remaining units remain passive. For both strategies we evaluate performance at three actuation levels corresponding

to low (300 µs), medium (500 µs), and high (700 µs) throttle for the BµBL platform. We measure the steady swimming speed of the aggregate and the electrical power consumed by the motor system of each BµBL in the aggregate. The motor system power is extracted from total power consumption by calibrating to a baseline power consumption measured when the robot is motionless – about 0.2 W. One complication is that chain aggregates are significantly less stable when all robots produce thrust compared to the rear-only propulsion strategy; as the chain of robots becomes longer, it is more susceptible to turn left or right rather than hold a straight heading. To address this, we employ local proportional-derivative control on robot attitude in the all-thrust case whereas the rear-only case is operated in open loop. Figure 6 shows the hardware configured in chains of one through five robots. Swimming efficiency was quantified using the cost of transport (CoT), which allows direct comparison between aggregate chains of different sizes:

$$\mathrm{CoT} = \frac{\sum_{i=1}^{N} P_i}{N\, m\, g\, v} \tag{1}$$

where $P_i$ is the average electrical power consumption of the $i^{th}$ BµBL propulsion system, $N$ is the number of robots in the chain, $g$ is gravity, $v$ is the steady-state velocity of the aggregate, and $m$ is the mass of a single BµBL. All BµBL robots are identical and have the same mass (127 g). Lower CoT indicates better swimming efficiency.

We find that the electrical power consumption of a BµBL propulsion system is approximately constant whether the robot operates individually or as part of an aggregate. Power consumption varies primarily with throttle level; robots draw between 3.5 W and 5.6 W depending on throttle setting and whether PD control or open-loop control is used. Figure 7 reports the swimming speed of one- through eight-robot chain aggregates under the all-thrust strategy, while Figure 8 reports the corresponding results for the rear-only thrust strategy. In the all-thrust case, aggregate speed monotonically increases with the number of participating robots, reaching a maximum of 41 cm/s, nearly an 80% increase relative to a single robot at 700 µs throttle. The relative speedup also depends on throttle level; at 500 µs throttle, an aggregate of eight robots swims approximately twice as fast as an individual robot. The rear-only thrust strategy results in aggregate speed decreasing with increasing chain length, however the relationship is not strictly monotonic and the speed decrease is relatively gradual. This mode produces highly efficient aggregate swimming because the chain morphology moves a large mass of robots for relatively little energy expenditure. Across all throttle levels, chain aggregates approach a CoT of approximately 2.0, compared to an individual BµBL which exhibits a CoT between 14.0 and 16.4 – more than 86% reduction. Figure 9 plots the 48 chain experiments on a CoT–speed diagram. Ellipses highlight the three clusters that emerge: the upper-left cluster corresponds to single-robot configurations, the lower-left cluster corresponds to rear-only multirobot chains, and the upper-right cluster corresponds to multirobot chains in which all BµBL robots generate thrust. These clusters show that chain aggregates access swimming regimes unavailable to a single robot. In particular, aggregates can move substantially faster at comparable CoT, or achieve much lower CoT at comparable speeds.

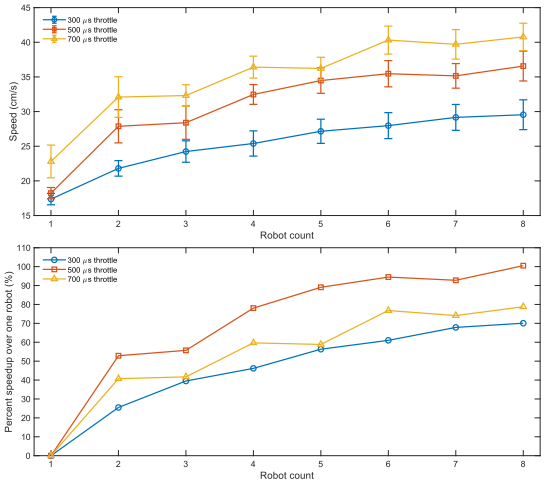


Fig. 7. All-thrust experiments: steady state speed measured for chain aggregates consisting of one to eight BµBL robots at three different throttle levels. Each robot in the chain is driven at equivalent thrust, and consumes an approximately equivalent amount of power. Error bars indicate one standard deviation in the instantaneous velocity measurements, as measured by frame-by-frame tracking in overhead video. The aggregates with eight robots swam the fastest in all cases, about 70 % to 100 % faster compared to an individual robot for the same power consumption per robot.

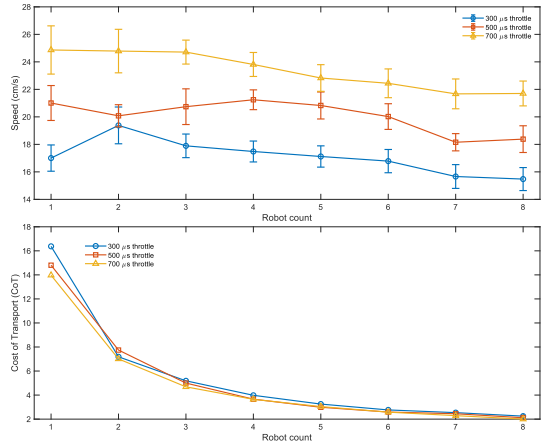


Fig. 8. Rear-only thrust experiments. Steady-state swimming speed and cost of transport (CoT) for chain aggregates consisting of one to eight BµBL robots at three throttle levels. CoT is computed from measured speed and electrical propulsion power according to Equation 1. As the number of robots in the chain increases, aggregate speed tends to decrease slightly. However, locomotion efficiency improves substantially as shown by a large reduction in CoT.

### *D. Distributed Sensing and Control*

To evaluate the benefits of distributed sensing and actuation, we develop a station-keeping experiment in which the performance of BµBL aggregates can be compared with that of an individual robot. The robot is tasked with maintaining

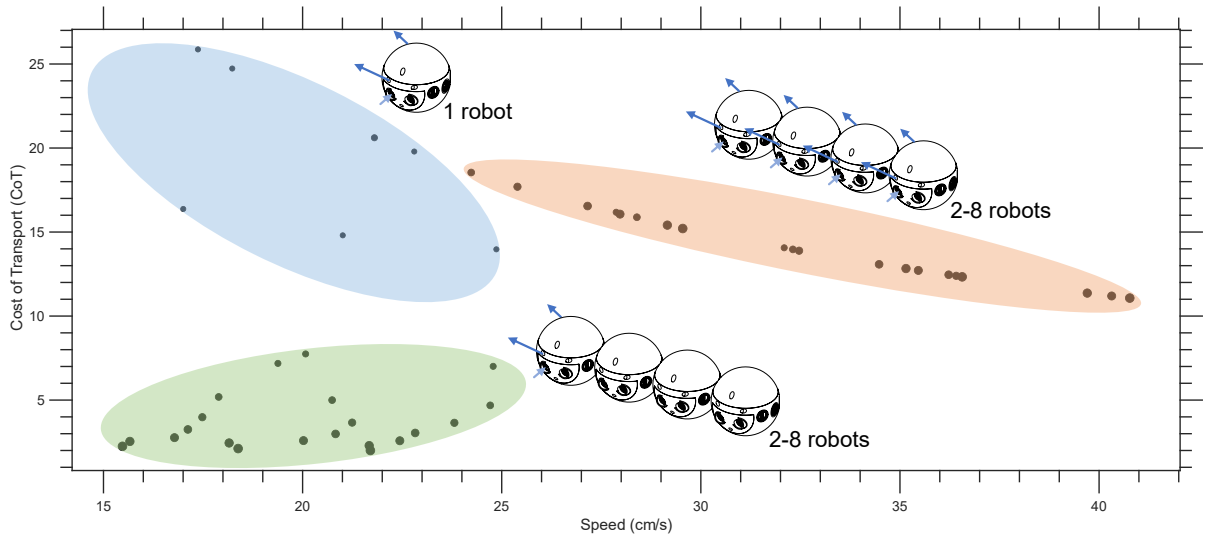


Fig. 9. CoT–speed plot summarizing all aggregate chain propulsion experiments. Each point represents a configuration for which steady swimming speed and electrical power were experimentally measured, and cost of transport (CoT) was computed from these measurements using Equation 1. Point size indicates the number of robots in the chain, with larger points corresponding to larger aggregates. Ellipses highlight three distinct clusters that emerge in the data. The upper-left blue cluster corresponds primarily to single-robot configurations (with one two-robot configuration), the lower-left green cluster corresponds to rear-only thrust chains with two or more robots, and the upper-right red cluster corresponds to all-thrust chains with two or more robots. The separation of these clusters illustrates how different propulsion strategies occupy distinct regions of the CoT–speed space. In particular, multi-robot aggregates reach performance regimes unavailable to a single robot, achieving substantially higher swimming speeds and lower cost of transport.

position relative to a red marker fixed to the wall of the tank. To accomplish this, the robot tracks the marker using its vision system and applies corrective yaw torques to keep the object centered in the image, along with forward or reverse thrust to maintain the desired distance. An individual robot struggles with this task due to limitations in both sensing and actuation. Over time, the robot develops oscillatory motion and lateral drift that it cannot compensate for because it can generate only weak lateral forces. In contrast, an aggregate of four robots arranged as shown in Figure 11 can produce strong lateral forces due to the perpendicular orientation of the robots in the aggregate. The aggregate also benefits from distributed sensing: four vision systems track four markers simultaneously rather than a single camera tracking one object. In both cases the robots execute identical control laws. The robots in the aggregate have no knowledge of their connectivity and do not communicate; instead they interact only through the forces and torques applied to the shared structure. These physical interactions are sufficient to maintain localization relative to the markers, effectively producing consensus through mechanical coupling. Results are summarized in Figure 12. Individual robots drift into the tank walls after less than $30\,\mathrm{s}$ of tracking, whereas the four-robot aggregate maintains position for substantially longer and with lower tracking error. These experiments demonstrate an architecture for mechanically coupled robot aggregates to parallelize sensing, computation, and actuation without explicit communication.

## IV. Conclusion

This paper explored colonial architectures for centimeter-scale underwater robots using magnetically docking modules capable of autonomous self-assembly and disassembly. Experiments showed that chain aggregates outperform individual robots both in terms of speed and cost of transport (CoT). When all robots apply thrust, chain aggregates swim substantially faster, reaching up to $41\,\mathrm{cm/s}$ in the eight robot case—nearly an 80% increase over a single robot. When only the rear robot provides thrust, locomotion efficiency improves dramatically, reducing cost of transport from 14–16 to approximately 2. A station-keeping experiment further illustrates how mechanically coupled aggregates can distribute sensing and actuation without explicit communication, enabling station-keeping behaviour that outperforms a single robot. These results suggest that colonial architectures of connected robot swarms can access performance regimes unavailable to individual robots. By exploiting self-reconfiguration, robot swarms can dynamically adjust their capabilities to match the task at hand. For example, robots may form aggregates to traverse long distances efficiently or generate higher thrust to overcome strong currents, and then disperse into individuals to cover larger areas during sensing or exploration (Figure 10). Even for a fixed size chain

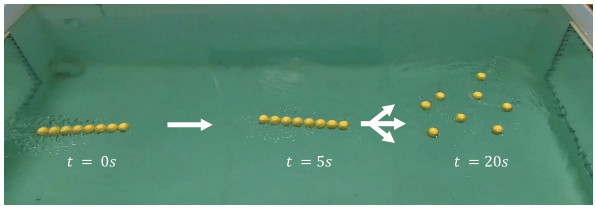


Fig. 10. A chain of eight BμBL robots traverses half of the tank as a chain aggregate and then self-disassembles into individual robots.

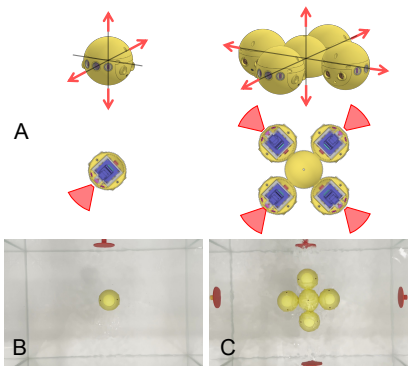


Fig. 11. (A) Distributed control experiment: a single robot lacks the ability to produce lateral thrusts as shown by the red translational degree of freedom arrows, and has a limited field of view as shown by the red cones. The aggregate 'X' structure by contrast can produce greater thrust in all directions, and has a much greater field of view. (B) Experiment setup for one robot. (C) Experiment setup for the multirobot aggregate.

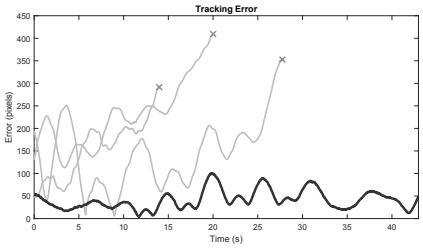


Fig. 12. Results of the station keeping experiment shown in Figure 11. The light grey curves show the tracking error over time for three experiments performed with an individual robot. The trajectories end when the robot collides with the tank wall. The bold curve shows the performance of the aggregate structure.

morphology, multiple propulsion strategies are possible due to the overactuation of the system. In this work we examined only two extreme cases—uniform thrust across all robots and rear-only propulsion—but many intermediate strategies exist in which subsets of robots generate thrust or thrust is distributed non-uniformly across the chain. Exploring these intermediate control regimes may reveal additional trade-offs between speed, efficiency, and maneuverability.

These results highlight several opportunities for future research. Better understanding the fluid interactions among distributed propulsors may inform new control strategies for coordinating thrust across aggregates. This work also did not explore optimal aggregate control; in all experiments, control of robot aggregates was accomplished through each robot executing its own series of proportional-derivative controllers with only local sensing and this was in many ways limiting. Multirobot control would benefit by taking advantage of the sensing of all robots in the aggregate and better coordination of the collective propulsors. Future work will investigate how the sensing, computing, and actuation resources of connected swarms can be synthesized under minimal communication so that the collective behaves as a single coordinated system.

## APPENDIX

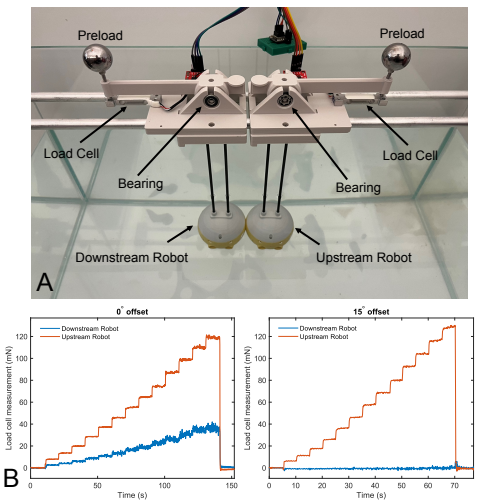


Fig. 13. (A) The thrust stand built to measure small coupling forces between robots, due to the downwash from an upstream robot interacting with the downstream robot. (B) Force-time plots of thrust experiments before and after $15^{\circ}$ degree corrections to the outlet vector. Without this correction, a component of the force generated by upstream robots appears as added drag on downstream robots, which reduces the aggregate net thrust.

## ACKNOWLEDGMENT

Pascal Spino is supported by a NASA Space Technology Graduate Research Opportunities Fellowship (NSTGRO) under grant number 80NSSC25K0239. The authors acknowledge the SMART M3 program and ONR Science of Autonomy under grant number N00014-23-1-2354.

## REFERENCES

[1] P. Wang, X. Liu, and A. Song, "Actuation and locomotion of miniature underwater robots: A survey," *Engineering (Beijing)*, Dec. 2024.

[2] T. Liu, Y. Liu, R. Zeng, B. Gan, M. Zhang, H. Li, S. Qu, and H. Zhou, "A bioinspired multimotion modality underwater microrobot," *Science Advances*, vol. 11, no. 19, May 2025. [Online]. Available: http://dx.doi.org/10.1126/sciadv.adu2527

[3] K. Li, X. Zhou, Y. Liu, J. Sun, X. Tian, H. Zheng, L. Zhang, J. Deng, J. Liu, W. Chen, and J. Zhao, "A 5 cm-scale piezoelectric jetting agile underwater robot," *Advanced Intelligent Systems*, vol. 5, no. 4, Jan. 2023. [Online]. Available: http://dx.doi.org/10.1002/aisy.202200262

[4] E. W. Schaler, M. Reinders, M. Holst, H. J. Lee, M. Samnani, T. Schafer, J. Holland, K. Bhingradiya, B. Liang, J. Vizcarra, J. Izraelevitz, S. Howell, E. Lesage, Z. Hao, and A. Ansari, "Design and development of swim – miniature, untethered underwater robots for exploring ice-ocean interfaces," in *2024 IEEE Aerospace Conference*, vol. 1. IEEE, Mar. 2024, p. 1–20. [Online]. Available: http://dx.doi.org/10.1109/AERO58975.2024.10521345

[5] A. B. Phillips, M. Haroutunian, S. K. Man, A. J. Murphy, S. W. Boyd, J. I. Blake, and G. Griffiths, *Nature in engineering for monitoring the oceans: comparison of the energetic costs of marine animals and AUVs*. Institution of Engineering and Technology, Jan. 2012, p. 373–405. [Online]. Available: http://dx.doi.org/10.1049/PBCE077E_ch17

[6] R. Bale, M. Hao, A. P. S. Bhalla, and N. A. Patankar, "Energy efficiency and allometry of movement of swimming and flying animals," *Proceedings of the National Academy of Sciences*, vol. 111, no. 21, p. 7517–7521, May 2014. [Online]. Available: http://dx.doi.org/10.1073/pnas.1310544111

[7] K. R. Sutherland and L. P. Madin, "Comparative jet wake structure and swimming performance of salps," *Journal of Experimental Biology*, vol. 213, no. 17, pp. 2967–2975, Sep. 2010. [Online]. Available: http://dx.doi.org/10.1242/jeb.041962

[8] A. Damian-Serrano, K. A. Walton, A. Bishop-Perdue, S. Bagoye, K. T. Du Clos, B. J. Gemmell, S. P. Colin, J. H. Costello, and K. R. Sutherland, "Colonial architecture modulates the speed and efficiency of multi-jet swimming in salp colonies," *Journal of Experimental Biology*, vol. 228, no. 6, Mar. 2025. [Online]. Available: http://dx.doi.org/10.1242/jeb.249465

[9] K. R. Sutherland and D. Weihs, "Hydrodynamic advantages of swimming by salp chains," *Journal of The Royal Society Interface*, vol. 14, no. 133, p. 20170298, Aug. 2017. [Online]. Available: http://dx.doi.org/10.1098/rsif.2017.0298

[10] K. T. Du Clos, B. J. Gemmell, S. P. Colin, J. H. Costello, J. O. Dabiri, and K. R. Sutherland, "Distributed propulsion enables fast and efficient swimming modes in physonect siphonophores," *Proceedings of the National Academy of Sciences*, vol. 119, no. 49, Nov. 2022. [Online]. Available: http://dx.doi.org/10.1073/pnas.2202494119

[11] Q. Bone and P. Anderson, "Communication between individuals in salp chains," *Proceedings of the Royal Society of London. Series B. Biological Sciences*, vol. 210, no. 1181, p. 559–574, Nov. 1980. [Online]. Available: http://dx.doi.org/10.1098/rspb.1980.0153

[12] G. O. MACKIE and Q. BONE, "Locomotion and propagated skin impulses in salps (tunicata: Thaliacea)," *The Biological Bulletin*, vol. 153, no. 1, p. 180–197, Aug. 1977. [Online]. Available: http://dx.doi.org/10.2307/1540700

[13] A. Damian-Serrano and K. R. Sutherland, "A developmental ontology for the colonial architecture of salps," *The Biological Bulletin*, vol. 245, no. 1, p. 9–18, Aug. 2023. [Online]. Available: http://dx.doi.org/10.1086/730459

[14] K. R. Sutherland, B. J. Gemmell, S. P. Colin, and J. H. Costello, "Propulsive design principles in a multi-jet siphonophore," *Journal of Experimental Biology*, Jan. 2019. [Online]. Available: http://dx.doi.org/10.1242/jeb.198242

[15] F. Berlinger, M. Gauci, and R. Nagpal, "Implicit coordination for 3d underwater collective behaviors in a fish-inspired robot swarm," *Science Robotics*, vol. 6, no. 50, 2021, cover Article –Movies – Focus and Science news.

[16] S. Mintchev, E. Donati, S. Marrazza, and C. Stefanini, "Mechatronic design of a miniature underwater robot for swarm operations," in *2014 IEEE International Conference on Robotics and Automation (ICRA)*, 2014, pp. 2938–2943.

[17] M. Yim, D. Duff, and K. Roufas, "Polybot: a modular reconfigurable robot," in *Proceedings 2000 ICRA. Millennium Conference. IEEE International Conference on Robotics and Automation. Symposia Proceedings (Cat. No.00CH37065)*, ser. ROBOT-00, vol. 1. IEEE, 2000, p. 514–520. [Online]. Available: http://dx.doi.org/10.1109/ROBOT.2000.844106

[18] C. McGray and D. Rus, "Self-reconfigurable molecule robots as 3d metamorphic robots," in *Proceedings. 1998 IEEE/RSJ International Conference on Intelligent Robots and Systems. Innovations in Theory, Practice and Applications (Cat. No.98CH36190)*, ser. IROS-98, vol. 2. IEEE, 1998, p. 837–842. [Online]. Available: http://dx.doi.org/10.1109/IROS.1998.727303

[19] J. W. Romanishin, K. Gilpin, and D. Rus, "M-blocks: Momentum-driven, magnetic modular robots," in *2013 IEEE/RSJ International Conference on Intelligent Robots and Systems*. IEEE, Nov. 2013, p. 4288–4295. [Online]. Available: http://dx.doi.org/10.1109/IROS.2013.6696971

[20] J. Romanishin, J. M. Bern, and D. Rus, "Self-reconfiguring robotic gantries powered by modular magnetic lead screws," in *2022 International Conference on Robotics and Automation (ICRA)*. IEEE, May 2022, p. 4225–4231. [Online]. Available: http://dx.doi.org/10.1109/ICRA46639.2022.9811863

[21] G. Liang, H. Luo, M. Li, H. Qian, and T. L. Lam, "Freebot: A freeform modular self-reconfigurable robot with arbitrary connection point - design and implementation," in *2020 IEEE/RSJ International Conference on Intelligent Robots and Systems (IROS)*. IEEE, Oct. 2020, p. 6506–6513. [Online]. Available: http://dx.doi.org/10.1109/IROS45743.2020.9341129

[22] P. Swissler and M. Rubenstein, "Fireantv3: A modular self-reconfigurable robot toward free-form self-assembly using attach-anywhere continuous docks," *IEEE Robotics and Automation Letters*, vol. 8, no. 8, p. 4911–4918, Aug. 2023. [Online]. Available: http://dx.doi.org/10.1109/LRA.2023.3290796

[23] C. Liu, Q. Lin, H. Kim, and M. Yim, "Smores-ep, a modular robot with parallel self-assembly," *Autonomous Robots*, vol. 47, no. 2, p. 211–228, Dec. 2022. [Online]. Available: http://dx.doi.org/10.1007/s10514-022-10078-1

[24] H. Wei, Y. Cai, H. Li, D. Li, and T. Wang, "Sambot: A self-assembly modular robot for swarm robot," in *2010 IEEE International Conference on Robotics and Automation*. IEEE, May 2010, p. 66–71. [Online]. Available: http://dx.doi.org/10.1109/ROBOT.2010.5509214

[25] M. Dorigo, "Swarm-bot: an experiment in swarm robotics," in *Proceedings 2005 IEEE Swarm Intelligence Symposium, 2005. SIS 2005.* IEEE, 2005, p. 192–200. [Online]. Available: http://dx.doi.org/10.1109/SIS.2005.1501622

[26] D. Zhao, H. Luo, Y. Tu, C. Meng, and T. L. Lam, "Snail-inspired robotic swarms: a hybrid connector drives collective adaptation in unstructured outdoor environments," *Nature Communications*, vol. 15, no. 1, Apr. 2024. [Online]. Available: http://dx.doi.org/10.1038/s41467-024-47788-2

[27] Y. Ozkan-Aydin and D. I. Goldman, "Self-reconfigurable multilegged robot swarms collectively accomplish challenging terradynamic tasks," *Science Robotics*, vol. 6, no. 56, Jul. 2021. [Online]. Available: http://dx.doi.org/10.1126/scirobotics.abf1628

[28] V. Zykov, E. Mytilinaios, B. Adams, and H. Lipson, "Self-reproducing machines," *Nature*, vol. 435, no. 7039, p. 163–164, May 2005. [Online]. Available: http://dx.doi.org/10.1038/435163a

[29] A. Abdel-Rahman, C. Cameron, B. Jenett, M. Smith, and N. Gershenfeld, "Self-replicating hierarchical modular robotic swarms," *Communications Engineering*, vol. 1, no. 1, Nov. 2022. [Online]. Available: http://dx.doi.org/10.1038/s44172-022-00034-3

[30] M. Smith, A. Abdel-Rahman, and N. Gershenfeld, "Self-reconfigurable robots for collaborative discrete lattice assembly," in *2024 IEEE International Conference on Robotics and Automation (ICRA)*. IEEE, May 2024, p. 3624–3631. [Online]. Available: http://dx.doi.org/10.1109/ICRA57147.2024.10609866

[31] D. Saldana, B. Gabrich, G. Li, M. Yim, and V. Kumar, "Modquad: The flying modular structure that self-assembles in midair," in *2018 IEEE International Conference on Robotics and Automation (ICRA)*. IEEE, May 2018, p. 691–698. [Online]. Available: http://dx.doi.org/10.1109/ICRA.2018.8461014

[32] W. Wang, N. Hagemann, A. Gonzalez-Garcia, C. Ratti, and D. Rus, "Self-reconfiguring modular robotic boats," Jul. 2025. [Online]. Available: http://dx.doi.org/10.21203/rs.3.rs-6942560/v1

[33] J. Zheng, G. Dai, B. He, Z. Mu, Z. Meng, T. Zhang, W. Zhi, and D. Fan, "Modcube: Modular, self-assembling cubic underwater robot," 2024. [Online]. Available: https://arxiv.org/abs/2409.15627

[34] D. Wang, F. Zhang, S. Zhang, D. Liu, J. Li, W. Chen, J. Deng, and Y. Liu, "Miniature modular reconfigurable underwater robot based on synthetic jet," *Advanced Science*, vol. 11, no. 39, Aug. 2024. [Online]. Available: http://dx.doi.org/10.1002/advs.202406956

[35] Z. Yang, Y. Zhang, M. Herbert, M. A. Hsieh, and C. Sung, "Effect of jet coordination on underwater propulsion with the multi-robot salp system," in *2025 IEEE 8th International Conference on Soft Robotics (RoboSoft)*. IEEE, Apr. 2025, p. 1–8. [Online]. Available: http://dx.doi.org/10.1109/RoboSoft63089.2025.11020967

[36] K. R. Sutherland, L. P. Madin, and R. Stocker, "Filtration of submicrometer particles by pelagic tunicates," *Proceedings of the National Academy of Sciences*, vol. 107, no. 34, p. 15129–15134, Aug. 2010. [Online]. Available: http://dx.doi.org/10.1073/pnas.1003599107

[37] P. Spino and D. Rus, "Towards centimeter-scale underwater mobile robots: An architecture for capable μauvs," in *2024 IEEE International Conference on Robotics and Automation (ICRA)*. IEEE, May 2024, p. 1484–1490. [Online]. Available: http://dx.doi.org/10.1109/ICRA57147.2024.10610474

[38] ——, "Bμbl: A centimeter-scale underwater robot," in *International Symposium on Experimental Robotics (ISER)*, 2025, to appear.

[39] K. R. Sutherland, B. J. Gemmell, S. P. Colin, and J. H. Costello, "Maneuvering performance in the colonial siphonophore, nanomia bijuga," *Biomimetics*, vol. 4, no. 3, p. 62, Sep. 2019. [Online]. Available: http://dx.doi.org/10.3390/biomimetics4030062